Langmuir
Article
pubs.acs.org/Langmuir

Electrowetting on a Polymer Microlens Array

Maesoon Im, Dong-Haan Kim,† Joo-Hyung Lee, Jun-Bo Yoon, and Yang-Kyu Choi*

Department of Electrical Engineering, KAIST, 335 Gwahangno, Yuseong-gu, Daejeon 305-701, Republic of Korea. †Present address: Doosan Heavy Industries and Construction Co., Ltd., Seoul, Republic of Korea

Received April 5, 2010. Revised Manuscript Received May 5, 2010

This paper reports on the electrowetting behavior of a flexible poly(dimethylsiloxane) (PDMS) microlens array. A Cr and Au double-layered electrode was formed on an array of microlenses with diameters of 10 μm and heights of 13 μm. A deposition of parylene and a coating of Teflon were followed for electrical insulation as well as for enhancement of the hydrophobicity. On the nearly superhydrophobic microlens array surface, the electrowetting of a deionized water droplet was observed over the contact angle range of ~140° to ~58° by applying 0−200 V, respectively. The electrowetting phenomenon was reversible even in air environment with applied voltages of less than 100 V. The electrowetting on the microlens array surface lost its reversibility after the microlens array surface was completely wetted when the water meniscus touched the bottom of the microlens array. Analysis of meniscus shapes and net force direction follows to elucidate the reversibility. The convex curvature of the microlens caused gradual rather than abrupt impalement of water into the gap among the microlenses.

1. Introduction

Like a lotus leaf in nature, many kinds of superhydrophobic surfaces have been created for academic investigations and practical purposes.[1−5] In addition to the development of superhydrophobic surfaces, the switching of wettability[6−12] is a highly attractive topic of research due to its wide functional applications.[13−20] Surface hydrophobicity has been achieved through electrical, electrochemical, optical, thermal, mechanical, and environmental methods. Previous approaches were summarized as well in review papers.[11,12] Among various methods for wettability switching, electrowetting or electrowetting-on-dielectric (EWOD) is the most popular method to modulate the shape of a liquid droplet and to manipulate a liquid droplet on a hydrophobic surface for numerous practical applications.[16−24]

In the process of electrowetting, a liquid droplet undergoes an alteration in its contact angle when an external electric field is applied across a dielectric layer between a bottom electrode and the liquid droplet. The contact angle induced by electrowetting (θ_A) on a flat surface can generally be given by the Lippmann−Young equation,[17] $\cos\theta_A = \cos\theta_0 + (\varepsilon_r\varepsilon_0/2\gamma_{la}t)V_A^2$, where V_A is the applied potential across the dielectric layer, θ_0 is the equilibrium contact angle at $V_A = 0$ V, ε_r is the relative permittivity of the dielectric layer, ε_0 is the permittivity of vacuum, γ_{la} is the liquid−air interfacial tension, and t is the thickness of the dielectric layer. On the other hand, the force generated by the difference in surface tensions for droplet movement, F_A, can be computed[22] by $F_A \cong (1/2)\pi R\gamma_{la}(\cos\theta_A - \cos\theta_0)$, where R is the radius of the liquid droplet base. From the aforementioned equation, a larger force for droplet movement can be expected for a larger difference in the contact angle. For a boost in F_A, the contact angle difference between θ_A and θ_0 should be enhanced. However, θ_A cannot be decreased further simply by applying higher bias (V_A) due to the saturation[23] of electric charges on the surface, which is not yet clearly understood.

Alternatively, by utilizing patterned microstructures on a surface, the initial contact angle (θ_0) without electrowetting can be improved according to the following equation of the Cassie−Baxter model:[25] $\cos\theta_{CB} = r_f f\cos\theta_{flat} + f - 1$. In this equation, θ_{CB} is the contact angle in the Cassie−Baxter regime, r_f is the ratio of the actual contact area between the liquid and the surface to the projected area of that surface, f is the portion of the surface in contact with the liquid, and θ_{flat} is the contact angle on a flat surface of an identical material. Furthermore, when the surface of

*To whom correspondence should be addressed. Telephone: +82-42-350-3477. Fax: +82-42-350-8565. E-mail: ykchoi@ee.kaist.ac.kr.

(1) Feng, X.; Jiang, L. *Adv. Mater.* **2006**, *18*, 3063–3078.
(2) Roach, P.; Shirtcliffe, N. J.; Newton, M. I. *Soft Matter* **2008**, *4*, 224–240.
(3) Li, X.-M.; Reinhoudt, D.; Crego-Calama, M. *Chem. Soc. Rev.* **2007**, *36*, 1350–1368.
(4) Zhang, X.; Shi, F.; Niu, J.; Jiang, Y.; Wang, Z. *J. Mater. Chem.* **2008**, *18*, 621–633.
(5) Chhatre, S. S.; Choi, W.; Tuteja, A.; Park, K.-C.; Mabry, J. M.; McKinley, G. H.; Cohen, R. E. *Langmuir* **2010**, *26*(6), 4027–4035.
(6) Callies, M.; Quéré, D. *Soft Matter* **2005**, *1*, 55–61.
(7) Erbil, H. Y.; Demirel, A. L.; Avci, Y.; Mert, O. *Science* **2003**, *299*, 1377–1380.
(8) Yuan, J.; Liu, X.; Akbulut, O.; Hu, J.; Suib, S. L.; Kong, J.; Stellacci, F. *Nat. Nanotechnol.* **2008**, *3*, 332–336.
(9) Lee, J.; He, B.; Patankar, N. A. *J. Micromech. Microeng.* **2005**, *15*, 591–600.
(10) Liu, H.; Feng, L.; Zhai, J.; Jiang, L.; Zhu, D. *Langmuir* **2004**, *20*(14), 5659–5661.
(11) Gras, S. L.; Mahmud, T.; Rosengarten, G.; Mitchell, A.; Kalantar-zadeh, K. *ChemPhysChem* **2007**, *8*, 2036–2050.
(12) Verplanck, N.; Coffinier, Y.; Thomy, V.; Boukherroub, R. *Nanoscale Res. Lett.* **2007**, *2*, 577–597.
(13) Chiou, P. Y.; Park, S.-Y.; Wu, M. C. *Appl. Phys. Lett.* **2008**, *93*(22), 221110.
(14) Lee, J.; Kim, C.-J. *J. Microelectromech. Syst.* **2000**, *9*(2), 171–180.
(15) Yun, K.-S.; Cho, I.-J.; Bu, J.-U.; Kim, C.-J.; Yoon, E. *J. Microelectromech. Syst.* **2002**, *11*(5), 454–461.
(16) Lee, J.; Moon, H.; Fowlerb, J.; Schoellhammerc, T.; Kim, C.-J. *Sens. Actuators, A* **2002**, *95*(2−3), 259–268.
(17) Cho, S. K.; Moon, H.; Kim, C.-J. *J. Microelectromech. Syst.* **2003**, *12*(1), 70–80.
(18) Banpurkar, A. G.; Nichols, K. P.; Mugele, F. *Langmuir* **2008**, *24*(19), 10549–10551.
(19) Zhao, Y.; Cho, S. K. *Lab Chip* **2006**, *6*, 137–144.
(20) Shamai, R.; Andelman, D.; Berge, B.; Hayes, R. *Soft Matter* **2008**, *4*, 38–45.
(21) Pollack, M. G.; Fair, R. B.; Shenderov, A. D. *Appl. Phys. Lett.* **2000**, *77*(11), 1725–1726.
(22) Abdelgawad, M.; Freire, S. L. S.; Yang, H.; Wheeler, A. R. *Lab Chip* **2008**, *8*, 672–677.
(23) Moon, H.; Cho, S. K.; Garrell, R. L.; Kim, C.-J. *J. Appl. Phys.* **2002**, *92*(7), 4080–4087.
(24) Brunet, P.; Lapierre, F.; Thomy, V.; Coffinier, Y.; Boukherroub, R. *Langmuir* **2008**, *24*(19), 11203–11208.
(25) Cassie, A. B. D.; Baxter, S. *Trans. Faraday Soc.* **1944**, *40*, 546–551.

the patterned microstructures is completely wetted by an applied voltage, it is also able to induce a lower contact angle (θ_A) than a flat surface by following the Wenzel model,[26] expressed as $\cos\theta_W = r\cos\theta_{flat}$, where θ_W is the contact angle in the Wenzel regime and r is the roughness factor of the surface (the ratio of the real surface area to the projected surface area). Consequently, on a microstructured surface, a greater change in contact angle is achievable from the high initial contact angle (θ_{CB}) before the electric charge is saturated in the dielectric material.[27] Furthermore, initial contact angle can be estimated by analytical modeling and calculations of the fractional area of microstructure array, while the calculation of the fractional area (f) in nonuniform nanostructures is very difficult due to the high randomness of nanosized components. This predictable design is another benefit of electrowetting on microstructured surfaces.

Researchers have reported numerous phenomena of electrowetting on microstructured[28−31] or nanostructured[24,27,32−37] surfaces for a large shift in contact angle or for real-time dynamic tuning of the wetting.[38] However, previous phenomena of electrowetting on microstructured surfaces were irreversible with water droplets in air environment, even though some reversible electrowetting was observed in specific environments, for example, two-liquid systems such as dodecane/water[30] or dodecane/saline.[33] Also, irreversible electrowetting on microstructured surfaces[28−31] and reversible electrowetting on some nanostructured surfaces[24,27,36,37] were just qualitatively explained. However, those qualities of irreversibility and reversibility should be comprehensively studied for the optimal design of structured surfaces with predictable electrowetting behavior. In this work, we report reversible electrowetting on a surface of a polymer microlens array even in air environment as long as the Cassie−Baxter state prevails. The experimental results in this paper are a continuation of our previous work[39,40] regarding polymer microlens arrays. Additionally, with an analysis of the water meniscus among the structures, we discuss the reversibility of electrowetting on the microlens array surface.

We determine that a microlens array provides reversible electrowetting due to gradual wetting[33] coming from the convex-curved shape. The electrowetting behavior was reversible until the applied potential reached a threshold value. When the applied voltage was above the threshold, the electrowetting became irreversible due to the transition from the Cassie−Baxter state to the Wenzel state.

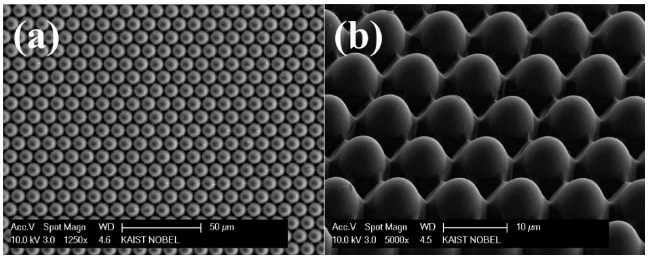

Figure 1. (a) Top view and (b) tilted view of scanning electron microscope photographs of the fabricated flexible microlens array.

2. Fabrication Process and Experimental Setup

A perfectly ordered microlens array was fabricated on a flexible substrate using three-dimensional diffuser lithography[41] and a replication process with a poly(dimethylsiloxane) (PDMS) elastomer.[39] A PDMS microlens array can be fabricated over a large area without any deposition and etching process. Inexpensive materials and simple lithography techniques enable a cost-effective and uniform creation of the microlens array even on a large area. Moreover, the repetitive use of the mold for the PDMS curing process can decrease the cost further. The detailed fabrication process of the PDMS microlens array is available in our previous reports.[39,40] As a bottom electrode layer used for electrowetting actuation, a double layer of Cr/Au (20 nm/300 nm) was sputtered on the fabricated PDMS microlens array. Onto the metal-sputtered PDMS microlens array, a 1 μm thick layer of parylene C was deposited with a parylene deposition system (PDS 2010 Labcoter 2; Speedline Technologies, Indianapolis, IN). The parylene C layer is used as a dielectric layer for electrical insulation between the liquid and the bottom electrode. To enhance the hydrophobicity of the microlens array surface,[39] an additional dielectric layer of 500 nm thick Teflon was coated by spinning 2 wt % Teflon AF2400 (amorphous fluoropolymer, DuPont, Wilmington, DE) solution dissolved in FC-40 (perfluorocarbon, 3M, St. Paul, MN) on the parylene layer. The final structure of the fabricated microlens array with an embedded metal electrode layer is shown in Figure 1. A single PDMS microlens had a diameter of 10 μm and a height of 13 μm before the dielectric layers were deposited. Compared with previous results,[39] the contact angle on the microlens array after parylene coating was decreased from 165° to 140° because the height of the PDMS microlens was reduced effectively by the additional thick parylene layer.

However, the hydrophobicity and hydrorepellency of the parylene-coated microlens array was confirmed by contact angle analysis to be superior to those characteristics of a flat Teflon surface. As shown in Movie S1 in the Supporting Information, a submergence test[42] in deionized water assures the stability of the hydrophobicity and hydrorepellency of the fabricated microlens array. Moreover, a larger initial contact angle than contact angle of the fabricated microlens array could be achieved by increasing the aspect ratio of the microlens array.[40] Superhydrophobicity dependence on the aspect ratio of microlens array has been reported in our previous work.[40]

As shown in Figure 2, the fabricated microlens array is highly flexible and does not lose its hydrophobicity and electrical connectivity even after a 10^5 cycle bending test.[39] On the PDMS microlens array, contact angle changes induced by electrowetting were analyzed and monitored with the measurement setup shown in Figure 3. By using a high voltage power supply that can provide up to 1000 V, a controlled voltage (V_A) was applied to the bottom

(26) Wenzel, R. N. *Ind. Eng. Chem.* **1936**, *28*(8), 988–994.
(27) Campbell, J. L.; Breedon, M.; Latham, K.; Kalantar-zadeh, K. *Langmuir* **2008**, *24*(9), 5091–5098.
(28) Herbertson, D. L.; Evans, C. R.; Shirtcliffe, N. J.; McHale, G.; Newton, M. I. *Sens. Actuators, A* **2006**, *130−131*, 189–193.
(29) Bhat, K.; Heikenfeld, J.; Agarwal, M.; Lvov, Y.; Varahramyan, K. *Appl. Phys. Lett.* **2007**, *91*(2), 024103.
(30) Zhou, K.; Heikenfeld, J. *Appl. Phys. Lett.* **2008**, *92*(11), 113515.
(31) Zhao, Y.; Chung, S. K.; Yi, U.-C.; Cho, S. K. *J. Micromech. Microeng.* **2008**, *18*, 025030.
(32) Krupenkin, T. N.; Taylor, J. A.; Schneider, T. M.; Yang, S. *Langmuir* **2004**, *20*(10), 3824–3827.
(33) Dhindsa, M. S.; Smith, N. R.; Heikenfeld, J.; Rack, P. D. *Langmuir* **2006**, *22*, 9030–9034.
(34) Zhu, L.; Xu, J.; Xiu, Y.; Sun, Y.; Hess, D. W.; Wong, C.-P. *J. Phys. Chem. B* **2006**, *110*(32), 15945–15950.
(35) Wang, Z.; Ou, Y.; Lu, T.-M.; Koratkar, N. *J. Phys. Chem. B* **2007**, *111*(17), 4296–4299.
(36) Verplanck, N.; Galopin, E.; Camart, J.-C.; Thomy, V.; Coffinier, Y.; Boukherroub, R. *Nano Lett.* **2007**, *7*(3), 813–817.
(37) Lapierre, F.; Thomy, V.; Coffinier, Y.; Blossey, R.; Boukherroub, R. *Langmuir* **2009**, *25*(11), 6551–6558.
(38) Heikenfeld, J.; Dhindsa, M. *J. Adhes. Sci. Technol.* **2008**, *22*, 319–334.
(39) Im, M.; Kim, D.-H.; Huang, X.-J.; Lee, J.-H.; Yoon, J.-B.; Choi, Y.-K. *Proceedings of the 22nd International Conference on Micro Electro Mechanical Systems*; IEEE: Sorrento, Italy, 2009.
(40) Huang, X.-J.; Kim, D.-H.; Im, M.; Lee, J.-H.; Yoon, J.-B.; Choi, Y.-K. *Small* **2009**, *5*(1), 90–94.
(41) Chang, S.-I.; Yoon, J.-B. *Opt. Express* **2004**, *12*, 6366–6371.
(42) Cao, L.; Hu, H.-H.; Gao, D. *Langmuir* **2007**, *23*(8), 4310–4314.

Figure 2. Photograph of the fabricated microlens array. The sample of the microlens array was bent for demonstration of flexibility.

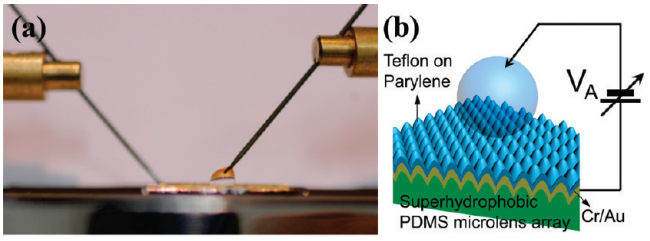

Figure 3. (a) Photograph of the setup for measurement of electrowetting responses. One probe was inserted into the droplet of deionized water, and the other probe touched the bottom electrode. (b) Experimental configuration for electrowetting and the cross section of the microlens array.

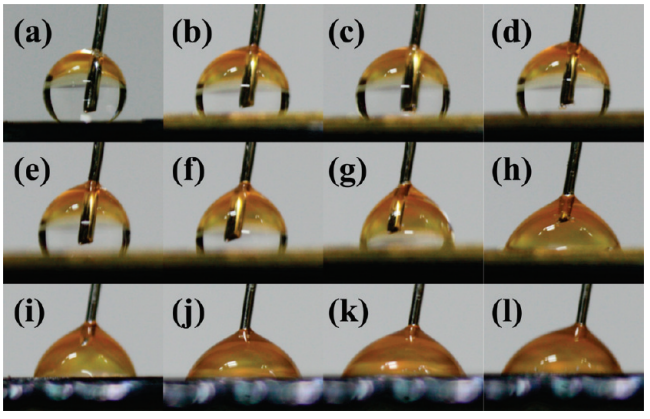

Figure 4. Optical images of shapes of the 10 μL deionized water. Applied voltages and contact angles were as follows: (a) 0 V, 140°; (b) 10 V, 119°; (c) 50 V, 117°; (d) 60 V, 115°; (e) 70 V, 111°; (f) 80 V, 98°; (g) 90 V, 91°; (h) 100 V, 78°; (i) 150 V, 77°; (j) 200 V, 58°; (k) 250 V, 58°; and (l) 300 V, 58°.

electrode underneath the parylene layer, while a deionized water droplet was grounded.

3. Results and Discussion

Figure 4 shows contact angle changes with various V_A values across the composite dielectric layer of parylene (1 μm) and Teflon (500 nm). All the contact angles were measured three times with the same conditions at room temperature. A huge contact angle change (82°) was achieved by electrowetting with an applied potential

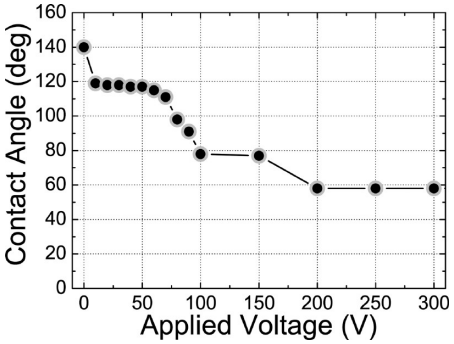

Figure 5. Dependence of the contact angle of deionized water on applied voltage. Electrolysis was observed when a voltage higher than 300 V was applied.

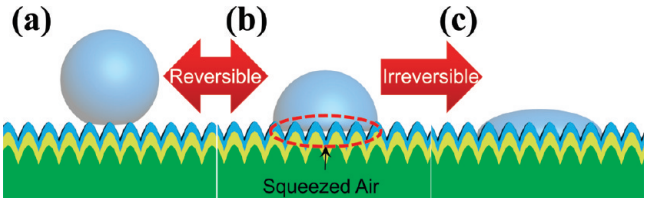

Figure 6. Diagrams illustrating three wetting states on a microlens array surface. (a) Initial Cassie−Baxter state without applied voltage. (b) Cassie−Baxter state with squeezed air by electrowetting. Until this state, contact angle change was reversible. (c) Wenzel state after complete wetting of the microlens array surface. After the threshold of transition from the Cassie−Baxter state to the Wenzel state, the contact angle change became irreversible.

between the droplet of deionized water and the bottom electrode. This amount of change in the contact angle is much higher than previous reversible electrowetting results on structured surfaces.[27,36,37] Moreover, reversibility is confirmed in a large range of 62°, from 140° to 78°, by applying 0−100 V, respectively. This contact angle change is the largest reversible one ever reported. The experimental contact angle changes are plotted in Figure 5. Whereas the Lippmann−Young equation is valid for a flat surface,[23] the electrowetting behavior on the microlens array does not follow the Lippmann−Young relationship.

As illustrated in Figure 6a, a water droplet on the fabricated microlens array without any electrical bias can be described by the Cassie−Baxter model. Although the water droplet was supported by the peaks of the microlens structures and air was trapped among the microlens structures, the Cassie−Baxter state was affected by external perturbation with an applied voltage of 10 V, and the trapped air began to be squeezed. Consequently, the contact angle of the water droplet decreased about 20°. Since the squeezed air resisted well against electrowetting until 50 V, as described in Figure 6b, there was a short plateau period showing small changes of contact angles in Figure 5. On the other hand, the higher potential evacuated air that is pressurized among the microlenses, and further gradual wetting, occurred reversibly until 100 V. Reversible electrowetting supports the idea that the Cassie−Baxter state is maintained so long as the applied bias is below 100 V. However, above 100 V, there was a final drop of contact angle at an applied bias of 200 V, and the microlens array surface was completely and irreversibly wetted, as shown in Figure 6c.

At low bias, it is believed that the supplied energy from electrowetting was consumed in pulling the water droplet into the air trapped region rather than in spreading the water over the surface. However, above a certain threshold bias, the water droplet was spread over neighboring microlenses to increase the base

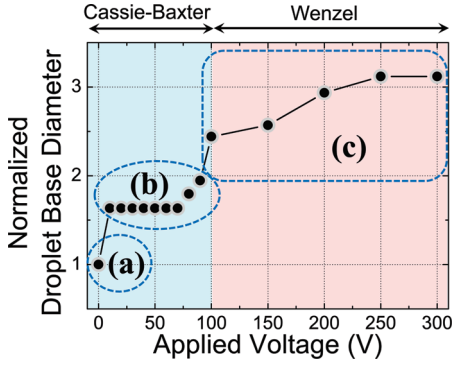

Figure 7. Change of the base diameter in a water droplet as a function of applied voltage. Diameters are normalized by the diameter of a water droplet without electrowetting. Wetting behaviors of (a−c) correspond to each letter of Figure 6. After complete penetration of water into the gaps among microlenses, the base diameter increased further by a lateral electrowetting.

diameter of the droplet. These behaviors were confirmed through the analysis of droplet base diameters, a process which was suggested by Herbertson et al.[28] In Figure 7, diameters are normalized by the diameter of a water droplet without electrowetting. As observed in Figure 7, the water droplet base widened suddenly at applied voltages near 10 and 100 V. These sudden increments of the base diameter gave evidence of the impalement of water inside gaps among microlens structures. Particularly, the final abrupt increment of droplet base at around 100 V implies the completed penetration of water. The base diameter analysis shows definitively that the electrowetting behavior of the droplet follows the Cassie−Baxter model until 100 V and that it follows the Wenzel model above 100 V. Due to the dielectric breakdown of the combined film of parylene C ($E_{breakdown}$ = 2 MV/cm)[29] and Teflon ($E_{breakdown}$ = 2 MV/cm),[23] electrolysis coming from dielectric breakdown was observed when a voltage greater than 300 V was applied to the system. In the case of dielectric breakdown, the sample cannot be used further for electrowetting due to the serious damage appearing as black scum.

On the surface of structures comprising vertical posts with a right side angle (90°), an abrupt change of the contact angle by electrowetting was observed.[32] In contrast, we expect reversible electrowetting on the microlens array that has sidewalls of a convex parabola shape, which may cause a gradual penetration of water. In the rest of this section, we will theoretically discuss the reason for gradual wetting and the threshold switching of the droplet's wetting states on the microlens array surface.

Wetting of a liquid droplet on a solid surface is a thermodynamic process. As shown in Figure 8a, the contact angle (θ_Y) on a planar surface is given by following Young's relation; $\gamma_{sa} = \gamma_{sl} + \gamma_{la} \cos \theta_Y$. Here, a liquid droplet is assumed to be in an air environment, γ_{sa} is the surface tension of the solid−air interface, γ_{sl} is the surface tension of the solid−liquid interface, and γ_{la} is the surface tension of the liquid−air interface. When the liquid droplet first contacts the surface, a composite interface composed of liquid, solid, and air is formed. As the droplet propagates on the surface texture, the original liquid−air interface and the air−solid interface are broken and replaced by a liquid−solid interface. Energy gain and loss happens in this process because some work over the aforementioned surface tensions (γ_{sa}, γ_{sl}, and γ_{la}) should be done to break the original composite interface. Equilibrium state is formed when the total energy reaches a minimum value.

As an electrical potential is applied to the electrowetting system, the charges are redistributed on the three-phase contact

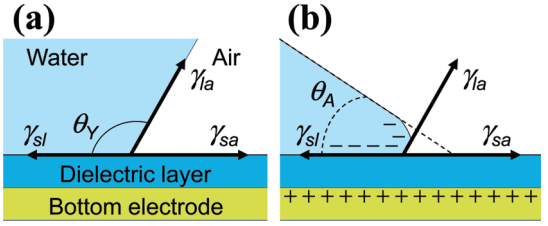

Figure 8. Schematic diagrams of the microscopic contact line on a flat hydrophobic surface: (a) at the initial state and (b) after electrowetting. Dashed line in (b) represents the macroscopic contact line.

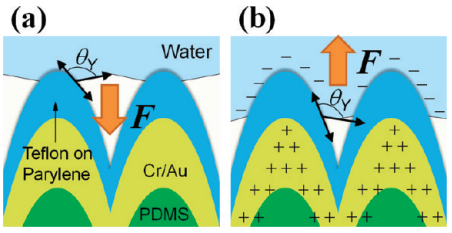

Figure 9. Schematic illustrations of the microscopic contact line and the water meniscus on the microlens array surface: (a) at the initial state and (b) after electrowetting. Note that the microscopic contact angle on the microlens surface is the same as the Young's contact angle (θ_Y) of 120° on a Teflon surface even after electrowetting. Initially, an upward meniscus generates a net force in a downward direction to assist electrowetting. As water penetrates into the space between microlenses by electrowetting, the meniscus becomes downward due to the geometrical shape of the microlens. Consequently, the net force in the upward direction prevents further impalement of water by additional electrowetting.

line, as depicted in Figure 8b, which causes noticeable wetting of liquid. It is noteworthy that, even though the macroscopic contact angle (θ_A) changes by electrowetting, the microscopic contact angle in the vicinity of the contact line is always equal to the Young's contact angle (θ_Y), regardless of applied voltage.[38,43] However, the slope of the water−air interface becomes lower than the slope in the initial state due to redistributed charges. This feature results in a reduction of the apparent contact angle.

This constant Young's contact angle and sidewall profile of the microlens provide a gradual wetting on the microlens array surface while electrowetting progresses by increasing electrical potentials. Due to the unique parabolic profile of the microlens sidewall,[44] the microscopic shape of the water meniscus is changed during the water impalement process enabled by electrowetting. Without any external bias, a water droplet is supported by the top surfaces of the microlens array as well as by the air trapped by adjacent microlenses. As illustrated in Figure 9a, the water droplet has an upward meniscus because the Young's contact angle is approximately 120° on a flat Teflon surface[39] and the sidewall has a gentle slope near the top of a microlens. Consequently, a net force (F) in the downward direction can be provided by the upward meniscus[38,42,45,46] to assist impalement of water with electrowetting. This analysis offers a clue to understand the large contact angle change with applied bias of 10 V, shown in Figure 5.

On the other hand, if water penetrates deeper into the space between microlenses by electrowetting, as shown in Figure 9b, the meniscus becomes downward due to the steeper slope of the

(43) Mugele, F.; Buehrle, J. *J. Phys.: Condens. Matter* **2007**, *19*, 375112.
(44) Chang, S.-I.; Yoon, J.-B.; Kim, H.; Kim, J.-J.; Lee, B.-K.; Shin, D. H. *Opt. Lett.* **2006**, *31*(20), 3016–3018.
(45) Tuteja, A.; Choi, W.; Mabry, J. M.; McKinley, G. H.; Cohen, R. E. *Proc. Nat.. Acad. Sci. U.S.A.* **2008**, *105*, 18200–18205.
(46) Im, M.; Im, H.; Lee, J.-H.; Yoon, J.-B.; Choi, Y.-K. *Soft Matter* **2010**, *6*(7), 1401–1404.

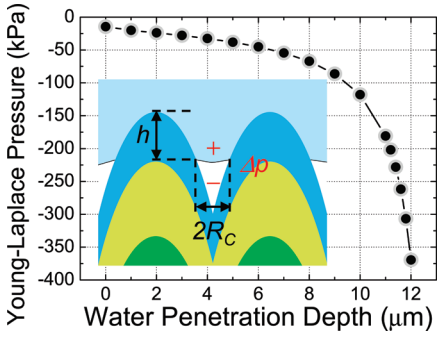

Figure 10. Plot of the Young−Laplace pressure (Δp) as a function of water penetration depth (h).

sidewall than the slope of the regions near the top of the microlens. As a result, the net force (F) is provided by the Young−Laplace pressure in the upward direction[38,42,45,46] and this pressure prevents further impalement of water by additional electrowetting. This effect provides the Cassie−Baxter state for reversible electrowetting and a small amount of changes in the contact angle. The result of the net force is implicitly expressed as a plateau, seen in Figure 5. Moreover, this resisting force is the reason for the threshold switching of the droplet's wetting states on the microlens array surface. Since the Young−Laplace pressure (Δp) is given by $\Delta p = 2\gamma_{la} \cos \theta_Y / R_C$,[47] where R_C is the radius of curvature of the water meniscus, the tendency of the Young−Laplace pressure on the microlens array as a function of penetration depth (h) of water can be estimated as shown in Figure 10. The radius of curvature of the water meniscus can be easily calculated from the parabolic relationship with penetration depth as $h = (13/25)(5\,\mu\text{m} - R_C)^2$ in the case of 10 μm diameter and 13 μm height of the microlens array. Figure 10 clearly shows that the Young−Laplace pressure hinders water penetration more as the water penetrates deeper into the microlens array. If a higher voltage than the threshold voltage is applied to the microlens array system, sufficient energy is supplied to exceed the antiwetting forces,[27] and the Wenzel state is achieved so that the water meniscus can reach the bottom of the microlens array. Then, electrowetting becomes irreversible.

Therefore, reversible electrowetting is primarily ascribed to gradual electrowetting on a microlens array surface due to the surface's inherent convex-curved shape. Despite better superhydrophobicity of a microbowl array surface[48] with its inherent concave-curved shape, which is a geometrical-complement pair of a microlens array suface,[40] that is, a "lock-and-key" structure, the structural material of PDMS and the dielectric layer were severely damaged by the strong electric field at the sharp peaks of the microbowl array with a metal electrode, when a much lower voltage is applied. This situation is not included in this work. As a consequence, electrowetting is expected to be impossible on a structured surface with concave-curved shapes fabricated with polymeric materials such as PDMS. Moreover, in the case of concave-shaped structures, it is obvious that the change in the net force by the Young−Laplace pressure becomes opposite against Figure 9. This feature may result in irreversible electrowetting due to the lack of gradual wetting.

4. Conclusion

Gradual electrowetting on a flexible polymer microlens array was demonstrated with large change of contact angle and reversible electrowetting behavior in a proper range of external bias. The parabolic convex profile of the microlens sidewall provided a downward shape of water meniscus as the electrowetting progresses. This downward meniscus supplies a net force through Young−Laplace pressure to resist against abrupt electrowetting by supporting a water droplet upward. Hence, the reversible electrowetting was attained on the fabricated flexible microlens array surface.

In previous works, the authors demonstrated the reduction of static friction force of a water droplet on a superhydrophobic microlens array by contact angle hysteresis analysis.[39] Additionally, the drag force reduction of the microlens array surface due to its microstructured features was also analyzed by simulations and experiments.[49] Therefore, with electrowetting, the microlens array surface is expected to be applicable to an effective system for liquid droplet manipulation. Moreover, due to the advantages of gradual electrowetting,[33] and due to the microlens structure, it is also expected that electrowetting on a microlens array surface with a transparent metal electrode can be utilized in various optical applications such as tunable optical lens,[20] electronic papers,[20,30,50] and so on.

Acknowledgment. This work was partially supported by a National Research Foundation of Korea (NRF) grant funded by the Korean Ministry of Education, Science and Technology (MEST) (No. 2009-0083079). It was also partially supported by the National Research and Development Program (NRDP, 2009-0065615) for the development of biomedical function monitoring biosensors, which was also funded by the Korean Ministry of Education, Science and Technology. M.I. would like to acknowledge the financial support of the Brain Korea 21 Project, in the School of Information Technology, KAIST, in 2009.

Supporting Information Available: Movie S1 is provided to demonstrate the hydrophobicity and hydrorepellency of the fabricated microlens array by a submergence test in deionized water. Also, Movie S2 is provided to show a reversible electrowetting on the fabricated microlens array by repetition of application and removal of 90 V. This material is available free of charge via the Internet at http://pubs.acs.org.

(47) Yun, K.-S.; Yoon, E.-S. *Biomed. Microdevices* **2005**, *7*, 35–40.
(48) Huang, X.-J.; Lee, J.-H.; Lee, J.-W.; Yoon, J.-B.; Choi, Y.-K. *Small* **2008**, *4*(2), 211–216.
(49) Im, M.; Im, H.; Kim, D.-H.; Lee, J.-H.; Yoon, J.-B.; Choi, Y.-K. *Proceedings of the 13th International Conference on Miniaturized Systems for Chemistry and Life Sciences*; The Chemical and Biological Microsystems Society: Jeju, Korea, 2009.
(50) Hayes, R. A.; Feenstra, B. J. *Nature* **2003**, *425*, 383–385.